Multifunctional Electronic Skin With a Stack of Temperature and Pressure Sensor Arrays

Yogeenth Kumaresan, Oliver Ozioko, and Ravinder Dahiya, *Fellow, IEEE*

***Abstract*—This paper presents multifunctional electronic skin (e-Skin) with a stack of pressure and temperature sensors arrays. The pressure sensor layer comprises of an 8x 8 array of capacitive sensors using soft elastomers as the dielectric medium and the temperature sensing layer comprises of 4 x4 array of conductive polymers based resistive sensors. Three variants of capacitive pressure sensors were developed using two different dielectric materials (PDMS and Ecoflex) to find the best combination of performance and softness. The Ecoflex-based pressure sensor showed high sensitivity (~4.11 kPa^{-1}) at a low-pressure regime (<1 kPa) and the 7.5:1 PDMS based pressure sensor showed high sensitivity (~2.32 kPa^{-1}) in the high-pressure regime (>1 kPa). Two variants of temperature sensors were fabricated using CNT and CNT & PEDOT:PSS conducting polymer composite and their performance compared. Finally, a highly sensitive CNT+PEDOT:PSS based resistive temperature sensors layer was integrated on top of 7.5:1 PDMS based capacitive pressure sensors layer to realize the e-Skin prototype. The developed e-Skin is capable of sensing pressures greater than 10 kPa with a high sensitivity of ~2.32 kPa^{-1} at 1 kPa and temperatures with the sensitivity of ~ 0.64 (%)/(°C) up to 80°C, thus demonstrating high potential for use in robotics and touch based interactive systems.**

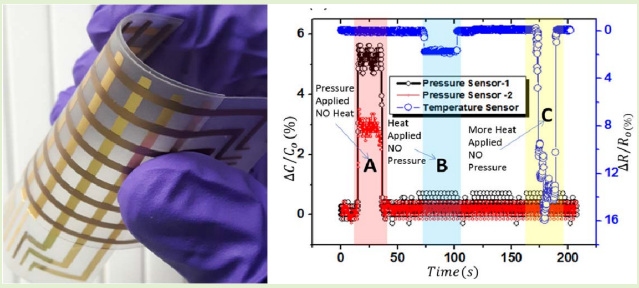

***Index Terms*—Touch sensors, e-Skin, temperature sensors, pressure sensors, flexible electronics, sensor stack.**

I. Introduction

THE electronic or tactile skin (e-Skin), composed of a variety of soft and flexible sensors, has been extensively investigated in recent years to bring the interactive artificial intelligent systems closer to mimicking the human skin [1]–[3]. For human skin-like functionality the e-Skin should allow to perceive and distinguish various spatiotemporal tactile stimuli such as pressure (static and dynamic), temperature, and strain etc., [4], [5]. This could enhance the granularity of the haptic information obtainable from e-Skin and could enable robots with human-like dexterity, cognitive skills, and abilities [4], [6]–[8]. The advantage of such e-Skin also expands to the provision of high-dimensional information from the environment for application in wearable health-monitoring system, smart phones, displays, and prosthetics [3], [4], [9], [10].

To mimic the functionality of human skin through electronics, it is necessary to understand its structure and various sensory receptors embedded in it [11], [12]. Human skin is capable of detecting multiple stimuli using different sensory receptors namely nociceptors, thermoreceptors, and mechanoreceptors that are embedded at different depths inside soft tissue [13], as shown in Fig. 1. Several variants of e-Skin have been reported with capability to measure a wide variety of stimuli such as pressure, temperature, proximity, slippage, object image, etc., [14], [15]. However, in contrast with human skin, most of the reported e-Skin solutions cannot detect more than one stimulus and normally it is the contact force. In this work, we present a multifunctional e-Skin with a stack of pressure and temperature sensors arrays. The pressure sensor layer comprises of an 8x 8 array of capacitive sensors and the temperature sensing layer comprises of 4 x4 array of conductive polymers based resistive sensors on flexible PVC substrate. This paper extends our preliminary results presented in IEEE FLEPS 2020 [16], [17]. The new results presented here are related to the fabrication and in-depth analysis of an array of capacitive pressure sensor, resistive temperature sensor and their integration as stack to detect both temperature

Manuscript received November 30, 2020; accepted January 15, 2021. Date of publication January 28, 2021; date of current version November 30, 2021. This work was supported in part by the Engineering and Physical Sciences Research Council (EPSRC) through Engineering Fellowship for Growth under Grant EP/M002527/1 and Grant EP/R029644/1 and in part by the European Commission through FET-OPEN Project Ph-Coding under Grant H2020- FETOPEN-2018-829186. This article was presented at the 2020 IEEE International Conference on Flexible and Printable Sensors and Systems (FLEPS). The associate editor coordinating the review of this article and approving it for publication was Prof. Arokia Nathan. *(Yogeenth Kumaresan and Oliver Ozioko contributed equally to this work.) (Corresponding author: Ravinder Dahiya.)*

The authors are with the Bendable Electronics and Sensing Technologies (BEST) Group, University of Glasgow, Glasgow G12 8QQ, U.K. (e-mail: ravinder.dahiya@glasgow.ac.uk).

This article has supplementary downloadable material available at https://doi.org/10.1109/JSEN.2021.3055458, provided by the authors.

Digital Object Identifier 10.1109/JSEN.2021.3055458

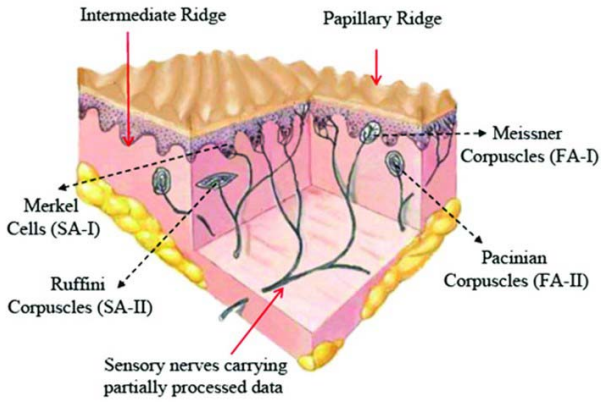

Fig. 1. A scheme showing the physical location of mechanoreceptors in Glabrous skin [13].

and pressure. The influence of the stiffness of dielectric medium on the performance of capacitive pressure sensor was carefully examined and the device-to-device variation in the array was investigated. Similarly, the in-depth analysis on reliability and cyclic performance of CNT+PEDOT:PSS resistive temperature sensor was investigated.

This paper is organized into four sections: The section II presents the state of art of pressure and temperature sensors. The fabrication process and integration of pressure and temperature sensors array as stack are discussed in Section III. The device characterization and related discussion are presented in Section IV. Finally, key findings are summarized in Section V.

II. State of the Art

A wider variety of pressure sensors using different transduction methods (e.g. capacitive, resistive, triboelectric, piezoresistive and piezoelectric etc.) have been reported for detection of static and dynamic forces and their locations [18]–[23]. Among them, vertically stacked capacitive pressure sensors are explored more due to advantages such as easy fabrication, stability, repeatability, and enhanced sensitivity for low ($<$10 kPa, mild touch) to high ($>$10 kPa, enabling object manipulation) pressure range, and simple readout electronics [24]. To enhance the sensitivity, researchers have explored various solutions such as using micro pillars, micro-cones, micro pyramid, micro cones, and/or bionic patterns etc., [25]–[30]. These approaches have yielded interesting results but understanding the role of dielectric material properties such as their stiffness is also an important factor that is needed to be explored to reproduce the mechanoreceptors sensing capability [16]. The latter is among the various investigations we have carried out in this work with capacitive pressure sensors using Ecoflex and PDMS as dielectric layers. Three different softness have been utilized to investigate the influence of dielectric property of materials and their stiffness.

The sensing functionality of thermoreceptors can be reproduced through sensors that measure the temperature either through a direct contact with the heat source or remotely through radiations. In this regard, various types of temperature sensors have been reported using mechanisms such as resistive, semiconductor, thermocouples, thermistor, and infrared etc. [31]–[35]. Among these the resistive type has been widely used due to the accuracy, stability, response time, and simple readout electronics [36]. The resistive sensors using materials such as carbon nanotube (CNT), poly (3,4- ethylenedioxythiophene): poly (styrene sulfonate) (PEDOT:PSS), graphene, and polymer composites etc. have been reported in the literature [37], [38]. However, many of these devices suffer from either slow recovery or response time, which limits their utilization in e-Skin. For example, the PEDOT:PSS based sensors demonstrate superior sensitivity to temperature but suffer from slow response and recovery time. On the contrary, the CNT based device demonstrate fast response and recovery time, but their response can be four times smaller than PEDOT:PSS [39], [40]. Such issues should be addressed to effectively utilize the temperature feedback in robotic applications. To this end, we have explored a mixture of CNT and PEDOT:PSS at 1:1 ratio as a sensing channel material and the results shows enhanced sensing response along with fast response and recovery time.

III. Materials and Methods

This section presents the materials and methods utilized for the realization of the multifunctional e-Skin which can respond to pressure (up to 160 kPa) and temperature (up to 80^{o}C). The commercially available flexible substrate namely polyvinyl chloride (PVC) with the thickness of $\sim$175μm was used as substrate for both the temperature and pressure sensors. The entire fabrication process is classified into three subsections: (1) a flexible pressure sensing array, (2) a temperature sensing array, and (3) the flexible e-Skin with integrated stack of pressure and temperature sensing arrays.

A. Fabrication of Flexible Pressure Sensor Array

For vertically stacked capacitive pressure sensor array, an elastomeric dielectric layer was sandwiched between two metal electrodes. Fig. 2a depicts the fabrication scheme of 8$\times$8 capacitive pressure sensor array. The top and bottom contact electrodes were fabricated by depositing titanium /gold (10/80nm thick Ti/Au) on a 175μm thick PVC substrate through a hard mask and electron-beam (e-beam) evaporator system. A computer-controlled blade cutter (Silhoutte Cameo) tool was used to realize the hard mask on PVC, which contains 8 parallel line openings with the line width, length, and pitch of 2mm, 6cm and 6mm respectively. Sequentially, a $\sim$125 μm thick dielectric elastomer was spin coated over bottom contact electrode; semi-cured at 60°C for $\sim$20 min; and top electrode was placed on directly on semi-cured elastomer. The line patterns of top and bottom electrodes were placed perpendicular to each other to obtain 8$\times$8 array (active area of single element is $\sim$2mm^2). We fabricated three sensor variants to evaluate the effect of dielectric property and the role of material stiffness on the sensor performance. The Ecoflex^{TM} with 1:1 mixing ratio of part A and B was used to fabricate sensor 1; PDMS elastomer and curing agent at 7.5:1 and 5:1 mixing ratios were utilized to fabricate sensor 2 and 3 respectively. A photographic image of 8$\times$8 pressure sensor array is shown in the left corner of Fig. 2a.

The capacitive pressure sensors were characterized by measuring the change in capacitance using a E4980AL precision LCR meter (Keysight Technologies, Santa Clara, CA,

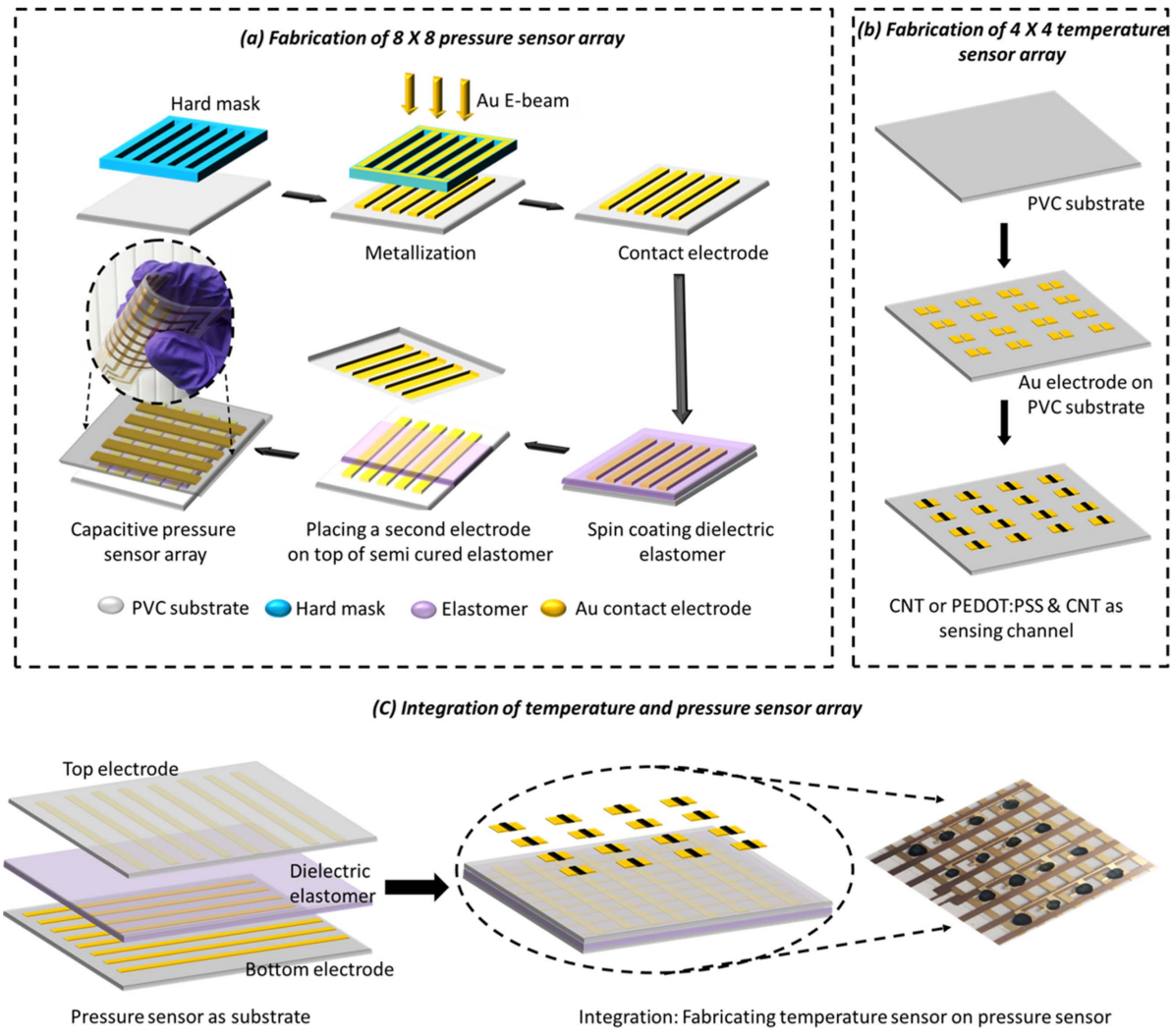

Fig. 2. A schematic representation of step-by-step fabrication of multifunctional e-Skin: (a) Fabrication of 8×8 capacitive pressure sensor array with dielectric elastomer placed between electrodes in vertical stacking arrangement; (b) fabrication of 4×4 temperature sensor array by drop casting active material (CNT or PEDO:PSS & CNT composite) over the contact electrodes; and (c) an integration of temperature and pressure sensor layers with former on the top.

USA) connected to a PC running a custom-made LabVIEW 2018 Robotics v18.0f2 (National Instruments, Texas, USA). Two set of experiments were conducted: one by varying the applied contact pressure (between 0 to 160 kPa) to investigate the sensitivity and another by applying a constant cyclic pressure of 7 kPa at 33Hz to investigate the sensor stability. For sensitivity study, the active device area of $\sim$1 cm^2 was fabricated because the large sensing area is preferable to obtain small pressure steps with respect to applied force (Pressure = Force / Area). All the sensors were firmly attached to a load cell made of 1004 aluminum and controlled pressure was applied through a plastic probe operated by computer-controlled linear stage with $\sim$0.1mm resolution.

B. Fabrication of Flexible Temperature Sensor Array

Fig. 2b shows the schematic process flow for fabrication of a 4×4 flexible temperature sensor array. The contact electrodes (10/80 nm thick Ti/Au) were deposited on PVC substrate using e-beam evaporator through hard mask that defines the channel length and width of 1mm and 2mm respectively. Two devices were fabricated using two sensing channel materials, namely single-walled CNT as sample 1 and PEDOT:PSS & single-walled CNT composite at 1:1 mixing ratio as sample 2. The channel material was drop-casted on the prefabricated electrodes and annealed at 80 °C for an hour. Finally, the sensing area was encapsulated with ultra-thin PDMS layer ($\sim$20μm thickness) by spin coating the 10:1 mixing ratio of elastomer and curing agent at 4000 rpm for 60 seconds to shield it against possible humidity. At the same time, the undesirable drop in temperature sensitivity due to thermally insulating PDMS encapsulation could be minimized by utilizing the ultra-thin layer. The temperature sensors were characterized by subjecting the sensors to temperature change using a hot plate and measuring the change in resistance of sensing channel region, using an Agilent 34461A digital multimeter connected to the sensor's contact.

C. Integration of Temperature and Pressure Sensor Array

Fig. 2c shows the integrated stack of temperature and pressure sensor layers. Firstly, 8×8 pressure sensor array was

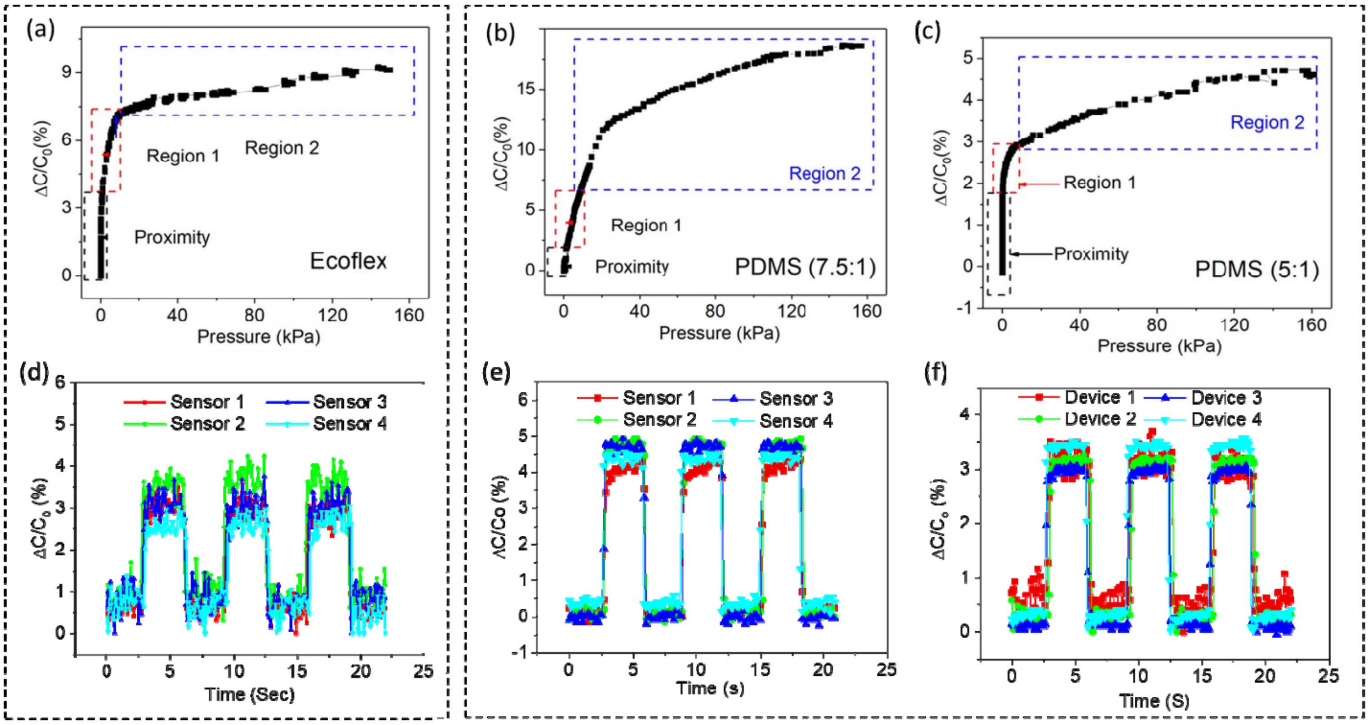

Fig. 3. Capacitive pressure sensor characteristics: (a-c) Relative capacitance change with respect to the applied pressure for (a) Ecoflex, (b) PDMS (7.5:1), and (c) PDMS (5:1) sensing layers; (d-f) time-resolved static capacitance change response under repeated mechanical loads for (d) Ecoflex, (e) PDMS (7.5:1), and (f) PDMS (5:1) sensing layers.

fabricated as described in section II(A). Sequentially, the temperature sensor was fabricated on top of the capacitive pressure sensor by following similar steps presented in section II (B). A photographic image of the multifunctional e-Skin with 8×8 pressure sensor array underneath the 4×4 temperature sensor array is shown in Fig. 2c. The performance of integrated sensor stack was tested using the designed readout electronics which uses Atmega 2560 microcontroller and analogue to digital converter (ADC) to identify different touch locations. Following this the pressure map was obtained using a computer.

IV. Results and Discussion

A. Pressure Sensor Characterization and Mapping

The performance of the capacitive pressure sensors based on different dielectric elastomers (Ecoflex and PDMS with two different stiffness) was evaluated by measuring the relative change in capacitance as shown in Fig. 3. The sensitivity of the pressure sensors was investigated by varying the applied contact pressure to a broad range varied from 0 to 160 kPa, which is 0 to 16 N force for 1 cm^2 device area (Fig. 3a-c). Considering the sense of touch and pressure experienced by the human skin, more than 90% of the mechanoreceptors are excited above 5 mN force [41], [42]. In general, the elastic deformation in the dielectric layer results in the change in capacitance value, which can be explained using parallel plate capacitor formula [43]; which shows that the capacitance is inversely proportional to the thickness of the dielectric material. As the sensors are subjected to the external pressure stimuli, the distance between the top and bottom contact electrodes decreases, and this results in an increase in capacitance value. Accordingly, the sensors revealed a capacitance change under applied pressure. In all the sensors, three regions with linear capacitance change were observed with sharp change at low pressure regions (proximity <1 kPa and region 1 between 1-10 kPa) and a gradual change at high pressure region (region 2 between 10-160 kPa) as shown in Fig. 3a-c. The sensitivity of the pressure sensor is given by [44]:

$$S = \delta(\Delta C/C_o)/\delta P \tag{1}$$

where P is the applied pressure, and $\Delta C/C_o$ ($\Delta C = C_{max} - C_o$) is relative change in capacitance in which C_o is initial capacitance and C_{max} is capacitance value under applied pressure. Fig. 4 displays the sensitivity of the pressure sensor at three regions extracted from relative capacitance change versus the applied pressure plot. At low-pressure range (<1 kPa), the Ecoflex based sensor (sensor 1) demonstrated highest sensitivity (4.11 kPa^{-1}) among all the other sensors. On the contrary, the PDMS based sensor (sensor 2) exhibited higher sensitivity of 1 kPa^{-1} in the region 1 (1-10 kPa) and 0.08 kPa^{-1} in the region 2 (10-160 kPa). This is due to the stiffness (Elastic modulus) of the dielectric elastomer that plays a vital role in determining the sensitivity of pressure sensors. For example, the Elastic modulus of Ecoflex, PDMS (7.5:1) and PDMS (5:1) are <0.1 MPa, 2.8 MPa and 3.5 MPa respectively [45], [46]. The material with low stiffness (low Elastic modulus) deforms faster than the high stiffness material. Therefore, the distance between the contact electrodes decreases faster and results in an increase in capacitive change (high sensitivity) at small pressure range for low stiffness material. Accordingly, the Ecoflex based sensor

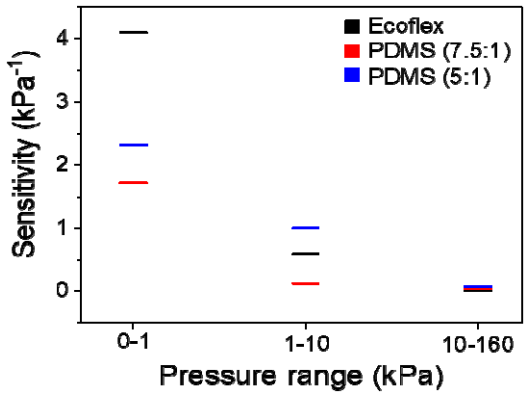

Fig. 4. Comparison of sensitivity under various pressure range (0-1 kPa, 1-10 kPa and 10-160 kPa) for sensor 1, sensor 2 and sensor 3.

revealed highest sensitivity at low pressure range making it suitable for light touch sensation. At the same time, Ecoflex (low stiffness) reaches deformation limit faster than the high stiffness PDMS. Therefore, the sensitivity of Ecoflex based sensor decreased at higher pressure region (region 1 and region 2) as shown in Fig 4. In case of high stiffness materials such as PDMS, the elastic deformation for low pressure range will be smaller and hence smaller change in capacitance is experienced, resulting in the lower sensitivity. Further, this material reaches its deformation limit at higher pressure range (>100 kPa). Therefore, reasonable deformation takes place for a broad pressure region (region 1 and region 2) until the elastomer reaches its maximum deformation limit. Likewise, the PDMS (7.5:1) based sensor revealed highest sensitivity in region 1 and region 2 making it a suitable material for higher stimulated pressure. However, when the stiffness of the material increases beyond certain limit, then negligible deformation will be observed in all the pressure ranges. Accordingly, the PDMS (5:1) that has the highest elastic modulus among all the sensors exhibited the lowest sensitivity in all the three regions due to negligible deformation.

A cyclic test was also performed, using four random sensing points on each of the 8×8 arrays to investigate their reliability and the device-to-device variation. This was carried out by applying cyclic loading (∼7 kPa) and unloading at every 0.33Hz frequency (Fig. 3d-e). All the three sensors demonstrated a quick response and recovery (<100 ms) with reliable performance. The calculated device to device variation on Ecoflex, PDMS (7.5:1) and PDMS (5:1) are 28 %, 14 % and 2244 % respectively. Based on these observations, the sensor 2 (using PDMS with the mixing ratio of 7.5:1), which demonstrated highest relative change in capacitance (∼5 %) at 7 kPa loading with minimum device to device variation (14 %), could be most suitable for pressure sensing over large area, as shown in supporting video S1. Further, the step response at low pressure range between 0 to 5kPa was performed on sensor 2. As shown in Fig. 5a, the sensor revealed a negligible hysteresis of less than 0.05%, which is extracted form relative chance in capacitance plot. In addition, sensor 2 exhibited stable performance under constant '1s' loading and '1s' unloading cycles for 500s (Fig. 5b). Therefore, sensor 2 was utilized for further studies.

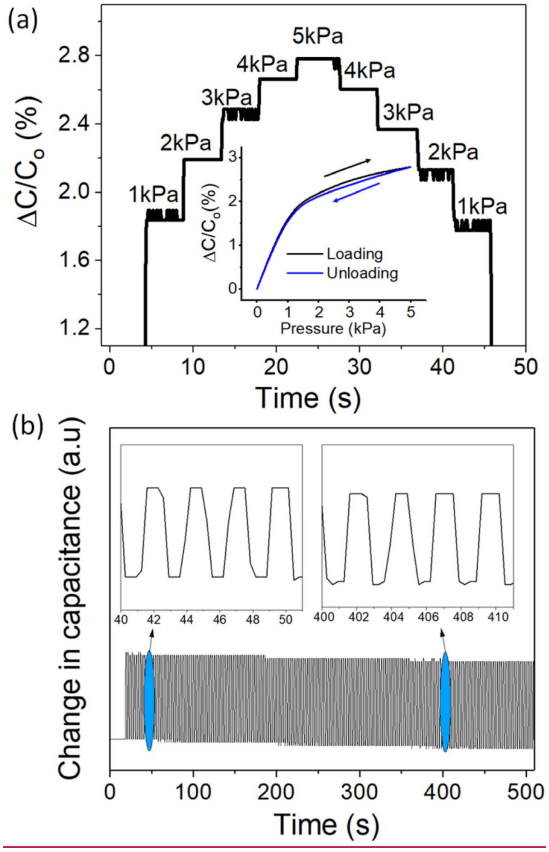

Fig. 5. Device reliability: (a) step response and hysteresis (inset) at 1kPa, 2kPa, 3kPA, 4kPa and 5kPA; (b) cyclic response with constant '1s' loading and '1s' unloading up to 250 cycles (500s) and their magnified graph (40-50s and 400-410s).

Fig. 6a shows the functional block diagram of the readout electronics designed for the fabricated pressure sensing array. The circuit was designed around a Microchip 8-bit Atmega 2560 AVR microcontroller with 256kB flash memory, a 10-bit 16-channel Analog to Digital Converter (ADC). The capacitance values of the sensors were recorded as a change in capacitance which occurs when the contacting point of each row (Tx lines) and column (Rx lines) representing each touch point is pressed. To efficiently read the capacitance values, we have utilized two CD74HC4051 - an 8-channel multiplexer allowing us to read both row and columns of the array. We tested the performance of the array using the designed readout electronics by touching different locations and recording the output of the Atmega 2560 and data was plotted as heat map (Fig. 6b-d) with blue as the least (not touched) and red representing absolute touch. The touch location and effect of proximity of the hand is shown by the colors of the different cells. To determine the exact location of the touch, a threshold was set to distinguish the individual touch events as represented by the different colors in Fig. 6b-d.

B. Temperature Sensor Characteristics

Fig. 7a and 7b show the time dependent response of CNT (sample 1) and PEDOT: PSS & CNT composite (sample 2) based temperature sensors. The temperature response was

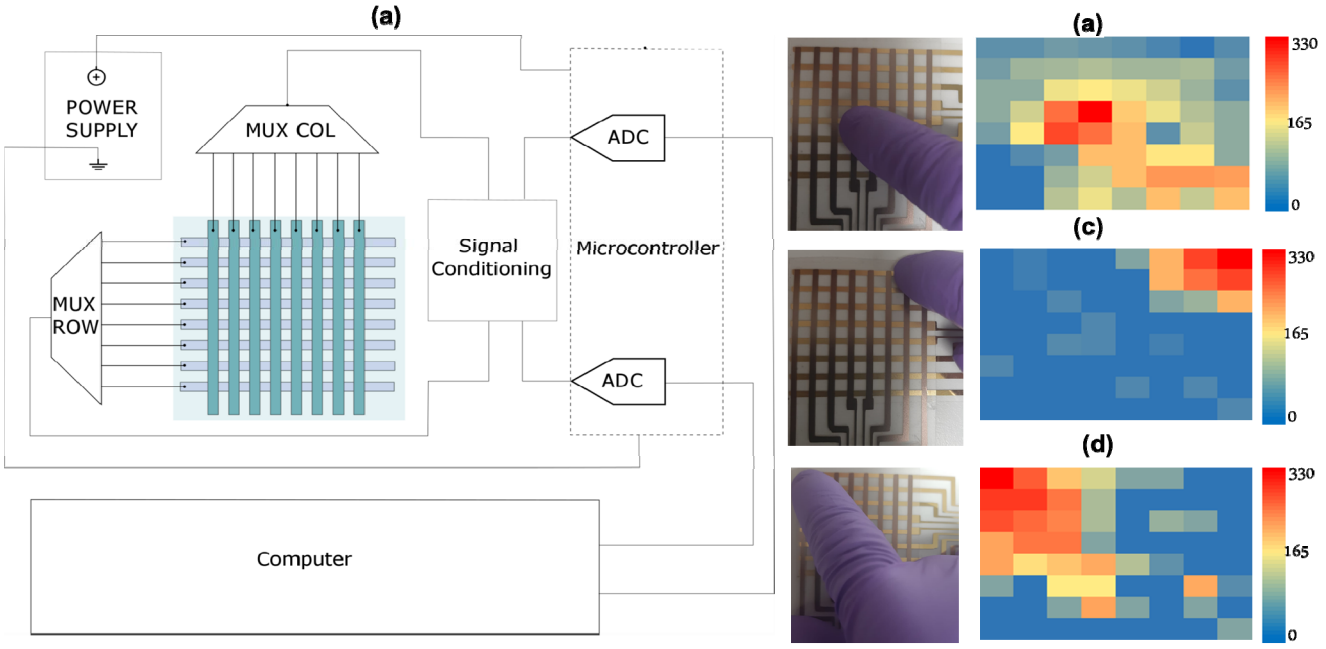

Fig. 6. (a) Functional block diagram pressure sensing array readout. (b) Performance of the pressure sensing array when touched at different locations.

recorded from room temperature (∼20 °C) by carefully placing the sensors on preheated hot plate maintained at different temperatures form 30-80 °C. Both sensors exhibited a negative temperature coefficient (NTC) of the resistance characteristics, with electrical resistance decreasing abruptly from 4700 Ω to 3900 Ω for sample 1 and 6150 Ω to 3300 Ω for sample 2. The relative change in resistance ($\Delta R/R_o$, where R_o is the base resistance and R is the sensor resistance) was extracted from the time dependent sensor plot. In the case of sample 1, a barrier exists at the interface between CNTs due to surface defects that provide a sustainable base resistance (∼ 4730 Ω) at room temperature [47]. With increasing temperature, the carrier concentration increases due to thermal fluctuations which assist the tunneling of carrier to eventually decrease the overall resistance [39], [48]. In case of sample 2, the PEDOT:PSS conducting polymer, which consist of conducting PEDOT core surrounded by the insulating PSS shell structure, provides an additional interface barrier to the CNTs and results in an increase of the base resistance (6150 Ω) (Fig. 7b). In general, the charge carrier generation and temperature response of PEDOT: PSS is better than the CNT [49], [50]. Therefore, with increase in temperature, both the CNT and PEDOT: PSS contributes to the charge carrier generation and transportation through hopping and tunneling mechanisms and result in huge drop in the resistance (two times higher than CNT). Accordingly, the sample 2 showed higher relative change in resistance than the sample 1 as can be seen in Fig. 7c. The response of sensors with respect to the change in temperature is plotted in the Fig. 7d. The response (%) is defined as 100 times the ratio of resistance changes after introducing temperature to the base resistance (the resistance at room temperature). In both sensors, the resistance value decreased linearly with increasing temperature. Thus, a linear increase in the response was observed. From Fig. 7d, the extracted sensitivity value for the sample 2 (∼0.64 (%)/(°C)) is 2.5 times higher than the sample 1 (∼0.27 (%)/(°C)).

Table I compares the performance of our sensor with the other state of the art sensors [17], [36], [49], [51], [52]. Further, the response and recovery behavior of our sensor is compared with commercialized thermistor in Fig. 8a. It is evident that our sensor demonstrated fast response and recovery behavior. This is because the temperature sensing phenomenon in most of the organic materials are based on the charge transportation through tunneling and hopping mechanism [36], [49]. Further, the presence of CNT in the organic material network introduces new percolation path for fast transportation of charge carrier [53]. As a result, the sample 2 with CNT in PEDOT: PSS network exhibited fast response (2.5 s) and recovery (4.8 s) behavior. Further, the reliability of the sample 2 was investigated by switching the sensor from 20 °C to 40 °C at every 30 s time interval for 7 cycles. As seen from Fig. 8b (supporting video S2), the CNT & PEDOT: PSS composite sensor demonstrated a stable and fast switching behavior useful to distinguish hot and cold objects. In addition, the sensor revealed negligible change in response under 40mm bending with the sensitivity of 0.64(%)/(°C) and 0.63(%)/(°C) at flat and bending condition (Fig. 8c).

C. Integration of Pressure and Temperature Sensor

Finally, we integrated both the pressure and temperature sensing layers to realize the stack capable of distinguishing both pressure and temperature. We utilized the pressure sensing array fabricated with 7.5:1 PDMS and the temperature sensing array realized with a composite of CNT & PEDOT: PSS. The e-Skin with integrated layers demonstrated a response similar to the independent temperature and pressure sensors. Further, the selectivity was good. Fig. 9

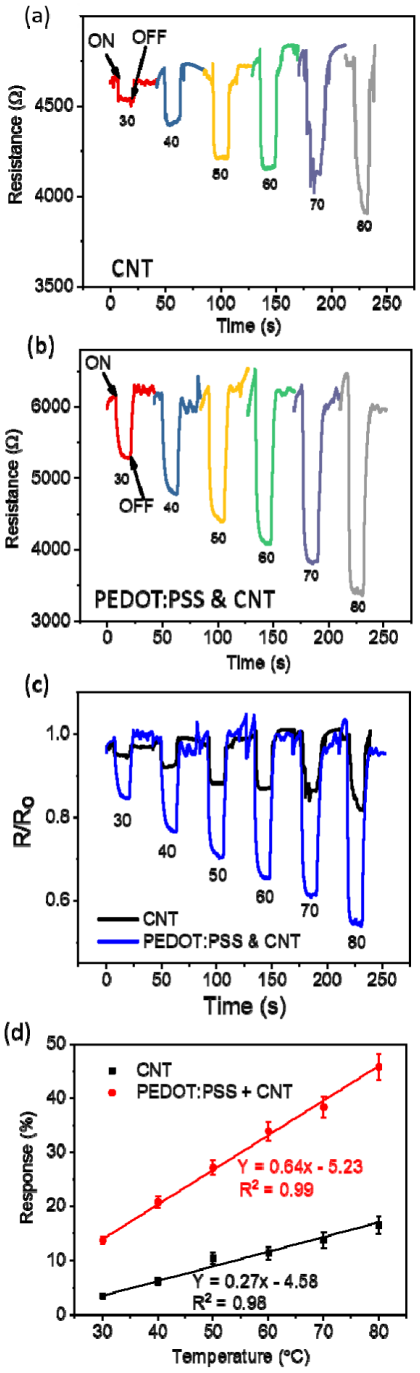

Fig. 7. Temperature sensor characteristics: Time-dependent temperature response of (a) sample 1 and (b) sample 2; The comparison of performance of sample 1 and sample 2 based on (c) relative change in resistance with respect to time and (d) their response (%) for temperature varied from 20 °C to 80 °C.

shows the investigation carried out to understand the capability of the integrated sensing stack to distinguish both pressure and temperature. To do this, we connected the array to the readout circuit described in Section III (A) (Fig. 5a) and output of the temperature sensor was read via the 10-bit analog channel of the microcontroller using a voltage divider configuration. Fig. 9a shows the location of the reference temperature sensor and the two pressure-sensitive pixels that were studied. Pressure was applied on point 1 and 2 (Fig. 9a) for ∼20s and the output of the temperature and pressure sensing array

TABLE I
TEMPERATURE SENSOR STATE OF ART

Sensing Material	*Sensitivity ($^0C^{-1}$)*	*Response Time*	*Recovery Time*	*Ref.*
GO + PEDOT:PSS	1.09	18 s for ΔT of 75 °C	32 s for ΔT of 75 °C	[36]
Reduced GO	0.6	1.2 s for ΔT of 20 °C	7 s for ΔT of 20 °C	[51]
Silver	0.2	-	-	[52]
PEDOT: PSS	0.48	-	-	[49]
CNT + PEDOT:PSS	**0.64**	**2.5s**	**4.8s**	**This work**

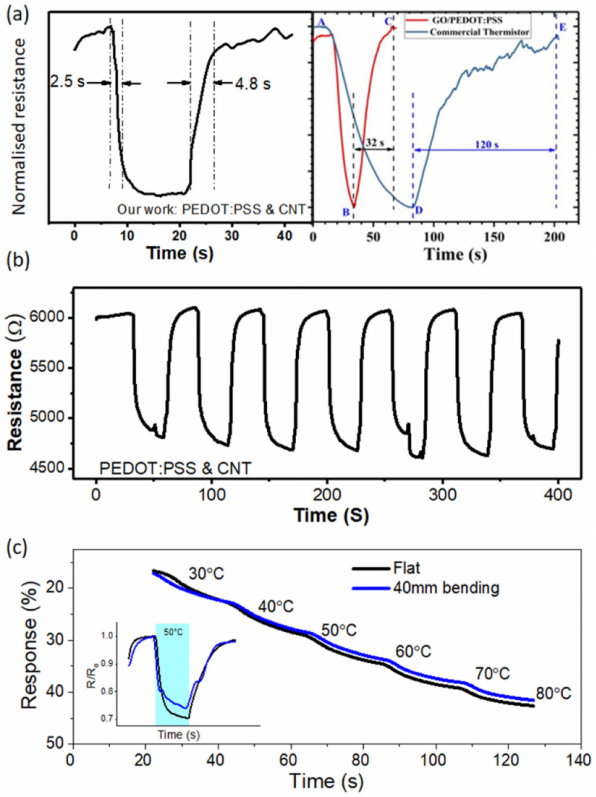

Fig. 8. (a) Comparison of response and recovery of our work with previous report [36]. The sensor response (normalised resistance) over time when transferred from 20 °C to 40 °C to highlight the response and recovery behavior. (b) Reliability test by cyclic switching of temperature from 20 °C to 40 °C at every 30 s for 7 min. Device flexibility test: (c) Step-response for temperature varied from 30 °C to 80 °C under flat and 40mm bending condition; inset shows time-dependent relative change in resistance at 50 °C.

was recorded simultaneously. The pressure was then released (for ∼30s) and heat was applied on the array using hot air gun from about 12cm distance for 30s and removed. After about 75s, more heat was applied to the array again for 20s with hot air gun from a closer distance (∼5cm). This was done to understand the response of integrated sensors at a higher temperature. Fig. 9b shows the result of the integrated array. Region A shows the period during which the pressure was applied. Both pressure sensors 1 and 2 responded with no significant change on the output of the temperature sensor. Heat was applied during the duration shown as region B. The outputs of both pressure sensors were relatively constant. This is same for region C when more heat was applied on the integrated array. Overall, it shows the capability of the

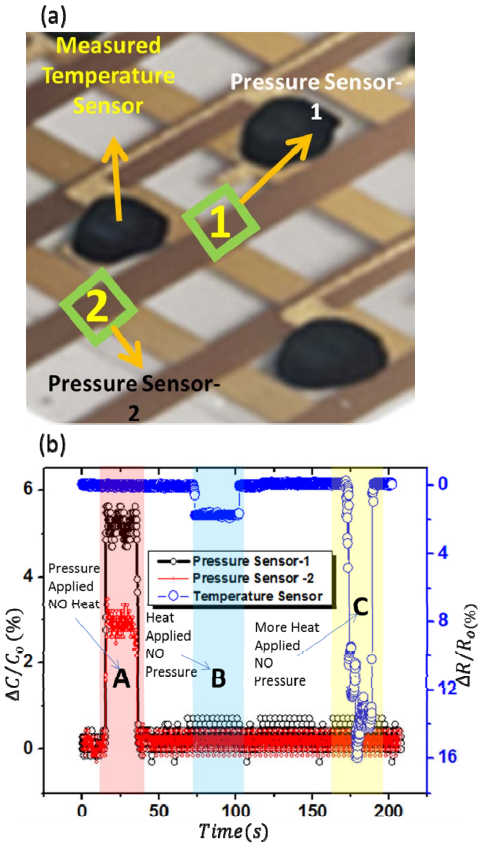

Fig. 9. (a) Reference pixels used during the characterization of the integrated temperature and pressure sensing array (b) Response of the integrated array to temperature and pressure.

integrated array to be able to distinguish both pressure and temperature with good selectivity.

V. Conclusion

We presented here the detailed steps for the realization of an e-Skin capable of detecting and distinguishing both pressure and temperature. Three different pressure sensors using PDMS of varying stiffness as well as Ecoflex were fabricated and characterized to choose optimal parameters. We also fabricated and compared two different temperature sensors using CNT and CNT & PEDOT: PSS composite as temperature sensing materials. The pressure and temperature sensors with optimal response were selected an integrated as stack to realize the e-Skin with temperature and pressure sensing capability. For pressure sensing array, we utilized PDMS with 7.5:1 ratio, and for temperature sensing array we utilized CNT+PEDOT: PSS based composite. The results show that the presented e-Skin patch is capable of sensing pressure >10kPa and temperature up to 80°C with fast response (2.5 s) and recovery (4.8 s) time - which is very good in comparison with state of the art. The integrated array presented here could act as the building block for multifunctional e-Skin suitable for application in robotics and touch based interactive systems. In future studies, the simultaneous operation of both the sensors (temperature and pressure) will be evaluated.

References

[1] S. Zhang, S. Li, Z. Xia, and K. Cai, "A review of electronic skin: Soft electronics and sensors for human health," *J. Mater. Chem. B*, vol. 8, no. 5, pp. 852–862, 2020.

[2] A. Shit, S. B. Heo, I. In, and S. Y. Park, "Mineralized soft and elastic polymer dot hydrogel for a flexible self-powered electronic skin sensor," *ACS Appl. Mater. Interfaces*, vol. 12, no. 30, pp. 34105–34114, Jul. 2020.

[3] P. Escobedo, M. Ntagios, D. Shakthivel, W. T. Navaraj, and R. Dahiya, "Energy generating electronic skin with intrinsic tactile sensing without touch sensors," *IEEE Trans. Robot.*, early access, Nov. 2, 2020, doi: 10.1109/tro.2020.3031264.

[4] M. Soni and R. Dahiya, "Soft eSkin: Distributed touch sensing with harmonized energy and computing," *Phil. Trans. Roy. Soc. A, Math., Phys. Eng. Sci.*, vol. 378, no. 2164, Feb. 2020, Art. no. 20190156.

[5] C. Zhang, S. Liu, X. Huang, W. Guo, Y. Li, and H. Wu, "A stretchable dual-mode sensor array for multifunctional robotic electronic skin," *Nano Energy*, vol. 62, pp. 164–170, Aug. 2019.

[6] R. Dahiya, D. Akinwande, and J. S. Chang, "Flexible electronic skin: From humanoids to humans," *Proc. IEEE*, vol. 107, no. 10, pp. 2011–2015, Oct. 2019.

[7] E. J. Markvicka, R. Tutika, M. D. Bartlett, and C. Majidi, "Soft electronic skin for multi-site damage detection and localization," *Adv. Funct. Mater.*, vol. 29, no. 29, Jul. 2019, Art. no. 1900160.

[8] X. Xun *et al.*, "Highly robust and self-powered electronic skin based on tough conductive self-healing elastomer," *ACS Nano*, vol. 14, no. 7, pp. 9066–9072, Jul. 2020.

[9] Y. Kumaresan *et al.*, "Omnidirectional stretchable inorganic-material-based electronics with enhanced performance," *Adv. Electron. Mater.*, vol. 6, no. 7, Jul. 2020, Art. no. 2000058.

[10] O. Ozioko, W. Navaraj, M. Hersh, and R. Dahiya, "Tacsac: A wearable haptic device with capacitive touch-sensing capability for tactile display," *Sensors*, vol. 20, no. 17, p. 4780, Aug. 2020.

[11] W. Gao *et al.*, "Fully integrated wearable sensor arrays for multiplexed *in situ* perspiration analysis," *Nature*, vol. 529, no. 7587, pp. 509–514, Jan. 2016.

[12] R. C. Webb *et al.*, "Ultrathin conformal devices for precise and continuous thermal characterization of human skin," *Nature Mater.*, vol. 12, no. 10, pp. 938–944, 2013.

[13] W. Navaraj and R. Dahiya, "Fingerprint-enhanced capacitive-piezoelectric flexible sensing skin to discriminate static and dynamic tactile stimuli," *Adv. Intell. Syst.*, vol. 1, no. 7, Nov. 2019, Art. no. 1900051.

[14] O. Ozioko, P. Karipoth, M. Hersh, and R. Dahiya, "Wearable assistive tactile communication interface based on integrated touch sensors and actuators," *IEEE Trans. Neural Syst. Rehabil. Eng.*, vol. 28, no. 6, pp. 1344–1352, Jun. 2020.

[15] G. Cheng, E. Dean-Leon, F. Bergner, J. R. G. Olvera, Q. Leboutet, and P. Mittendorfer, "A comprehensive realization of robot skin: Sensors, sensing, control, and applications," *Proc. IEEE*, vol. 107, no. 10, pp. 2034–2051, Oct. 2019.

[16] Y. Kumaresan, O. Ozioko, and R. Dahiya, "Effect of dielectric and stiffness of soft material between the electrodes of a capacitive pressure sensor on its performance," in *Proc. IEEE Int. Conf. Flexible Printable Sensors Syst. (FLEPS)*, Aug. 2020, pp. 1–4.

[17] O. Ozioko, Y. Kumaresan, and R. Dahiya, "Carbon nanotube/PEDOT: PSS composite-based flexible temperature sensor with enhanced response and recovery time," in *Proc. IEEE Int. Conf. Flexible Printable Sensors Syst. (FLEPS)*, Aug. 2020, pp. 1–4.

[18] L. Gao *et al.*, "All paper-based flexible and wearable piezoresistive pressure sensor," *ACS Appl. Mater. Interfaces*, vol. 11, no. 28, pp. 25034–25042, Jul. 2019.

[19] Y. Luo *et al.*, "Flexible capacitive pressure sensor enhanced by tilted micropillar arrays," *ACS Appl. Mater. Interfaces*, vol. 11, no. 19, pp. 17796–17803, May 2019.

[20] B. C.-K. Tee, A. Chortos, R. R. Dunn, G. Schwartz, E. Eason, and Z. Bao, "Tunable flexible pressure sensors using microstructured elastomer geometries for intuitive electronics," *Adv. Funct. Mater.*, vol. 24, no. 34, pp. 5427–5434, Sep. 2014.

[21] H. Liu *et al.*, "Stretchable conductive nonwoven fabrics with self-cleaning capability for tunable wearable strain sensor," *Nano Energy*, vol. 66, Dec. 2019, Art. no. 104143.

[22] N. Yogeswaran, E. S. Hosseini, and R. Dahiya, "Graphene based low voltage field effect transistor coupled with biodegradable piezoelectric material based dynamic pressure sensor," *ACS Appl. Mater. Interfaces*, vol. 12, no. 48, pp. 54035–54040, Dec. 2020, doi: 10.1021/acsami.0c13637.

[23] M. Ntagios, H. Nassar, A. Pullanchiyodan, W. T. Navaraj, and R. Dahiya, "Robotic hands with intrinsic tactile sensing via 3D printed soft pressure sensors," *Adv. Intell. Syst.*, vol. 2, no. 6, Jun. 2020, Art. no. 1900080.

[24] S. Wan *et al.*, "Graphene oxide as high-performance dielectric materials for capacitive pressure sensors," *Carbon*, vol. 114, pp. 209–216, Apr. 2017.
[25] S. C. B. Mannsfeld *et al.*, "Highly sensitive flexible pressure sensors with microstructured rubber dielectric layers," *Nature Mater.*, vol. 9, no. 10, pp. 859–864, Oct. 2010.
[26] C. M. Boutry *et al.*, "A hierarchically patterned, bioinspired e-skin able to detect the direction of applied pressure for robotics," *Sci. Robot.*, vol. 3, no. 24, Nov. 2018, Art. no. eaau6914.
[27] Y. Zhang *et al.*, "Dual-mode electronic skin with integrated tactile sensing and visualized injury warning," *ACS Appl. Mater. Interfaces*, vol. 9, no. 42, pp. 37493–37500, Oct. 2017.
[28] P. Nie *et al.*, "High-performance piezoresistive electronic skin with bionic hierarchical microstructure and microcracks," *ACS Appl. Mater. Interfaces*, vol. 9, no. 17, pp. 14911–14919, May 2017.
[29] H. Li, S. Lv, and Y. Fang, "Bio-inspired micro/nanostructures for flexible and stretchable electronics," *Nano Res.*, vol. 13, no. 5, pp. 1244–1252, May 2020.
[30] H. Niu, S. Gao, W. Yue, Y. Li, W. Zhou, and H. Liu, "Highly morphology-controllable and highly sensitive capacitive tactile sensor based on epidermis-dermis-inspired interlocked asymmetric-nanocone arrays for detection of tiny pressure," *Small*, vol. 16, no. 4, 2020, Art. no. 1904774.
[31] T. Q. Trung, S. Ramasundaram, B.-U. Hwang, and N.-E. Lee, "An all-elastomeric transparent and stretchable temperature sensor for body-attachable wearable electronics," *Adv. Mater.*, vol. 28, no. 3, pp. 502–509, Jan. 2016.
[32] Q. Liu, H. Tai, Z. Yuan, Y. Zhou, Y. Su, and Y. Jiang, "A high-performances flexible temperature sensor composed of polyethyleneimine/reduced graphene oxide bilayer for real-time monitoring," *Adv. Mater. Technol.*, vol. 4, no. 3, Mar. 2019, Art. no. 1800594.
[33] P. Tao *et al.*, "Bioinspired engineering of thermal materials," *Adv. Mater.*, vol. 27, no. 3, pp. 428–463, 2015.
[34] R. S. Dahiya *et al.*, "Towards tactile sensing system on chip for robotic applications," *IEEE Sensors J.*, vol. 11, no. 12, pp. 3216–3226, Dec. 2011.
[35] S. Hannah, A. Davidson, I. Glesk, D. Uttamchandani, R. Dahiya, and H. Gleskova, "Multifunctional sensor based on organic field-effect transistor and ferroelectric poly(vinylidene fluoride trifluoroethylene)," *Organic Electron.*, vol. 56, pp. 170–177, May 2018.
[36] M. Soni, M. Bhattacharjee, M. Ntagios, and R. Dahiya, "Printed temperature sensor based on PEDOT:PSS-graphene oxide composite," *IEEE Sensors J.*, vol. 20, no. 14, pp. 7525–7531, Jan. 2020.
[37] C. Bali, A. Brandlmaier, A. Ganster, O. Raab, J. Zapf, and A. Hübler, "Fully inkjet-printed flexible temperature sensors based on carbon and PEDOT: PSS," *Mater. Today Proc.*, vol. 3, no. 3, pp. 739–745, 2016.
[38] M. Bhattacharjee, M. Soni, P. Escobedo, and R. Dahiya, "PEDOT:PSS microchannel-based highly sensitive stretchable strain sensor," *Adv. Electron. Mater.*, vol. 6, no. 8, 2020, Art. no. 2000445.
[39] V. S. Turkani, D. Maddipatla, B. B. Narakathu, B. J. Bazuin, and M. Z. Atashbar, "A carbon nanotube based NTC thermistor using additive print manufacturing processes," *Sens. Actuators A, Phys.*, vol. 279, pp. 1–9, Aug. 2018.
[40] J. Štulík *et al.*, "Comparison of organic thermistors based on PEDOT:PSS and PEDOT:Tos thin films under various thermal and humidity conditions," *Sens. Actuators B, Chem.*, vol. 275, pp. 359–366, Dec. 2018.
[41] R. S. Johansson and A. B. Vallbo, "Detection of tactile stimuli. Thresholds of afferent units related to psychophysical thresholds in the human hand," *J. Physiol.*, vol. 297, no. 1, pp. 405–422, Dec. 1979.
[42] R. S. Dahiya and M. Valle, *Robotic Tactile Sensing: Technologies and System*. Amsterdam, The Netherlands: Springer, 2013.
[43] N. Ni and L. Zhang, "Dielectric elastomer sensors," in *Elastomers*, N. Cankaya, Ed. Rijeka, Croatia: IntechOpen, 2017.
[44] J. Yang, S. Luo, X. Zhou, J. Li, J. Fu, and W. Yang, "Flexible, tunable, and ultrasensitive capacitive pressure sensor with microconformal graphene electrodes," *ACS Appl Mater Interfaces*, vol. 11, no. 16, pp. 14997–15006, Mar. 2019.
[45] B. Wang, W. Huang, L. Chi, M. Al-Hashimi, T. J. Marks, and A. Facchetti, "High-*k* gate dielectrics for emerging flexible and stretchable electronics," *Chem. Rev.*, vol. 118, no. 11, pp. 5690–5754, 2018.
[46] Z. Wang, A. A. Volinsky, and N. D. Gallant, "Crosslinking effect on polydimethylsiloxane elastic modulus measured by custom-built compression instrument," *J. Appl. Polym. Sci.*, vol. 131, no. 22, Nov. 2014.
[47] A. Di Bartolomeo *et al.*, "Multiwalled carbon nanotube films as small-sized temperature sensors," *J. Appl. Phys.*, vol. 105, no. 6, Mar. 2009, Art. no. 064518.
[48] B. Monea *et al.*, "Single wall carbon nanotubes based cryogenic temperature sensor platforms," *Sensors*, vol. 17, no. 9, p. 2071, Sep. 2017.
[49] J.-W. Lee, D.-C. Han, H.-J. Shin, S.-H. Yeom, B.-K. Ju, and W. Lee, "PEDOT:PSS-based temperature-detection thread for wearable devices," *Sensors*, vol. 18, no. 9, p. 2996, Sep. 2018.
[50] Y.-F. Wang *et al.*, "Fully printed PEDOT:PSS-based temperature sensor with high humidity stability for wireless healthcare monitoring," *Sci. Rep.*, vol. 10, no. 1, p. 2467, Dec. 2020.
[51] G. Liu *et al.*, "A flexible temperature sensor based on reduced graphene oxide for robot skin used in Internet of Things," *Sensors*, vol. 18, no. 5, p. 1400, 2018.
[52] M. D. Dankoco, G. Y. Tesfay, E. Benevent, and M. Bendahan, "Temperature sensor realized by inkjet printing process on flexible substrate," *Mater. Sci. Eng. B*, vol. 205, pp. 1–5, Mar. 2016.
[53] J. Mannayil, S. M. Raman, J. Sankaran, R. Raman, and J. M. K. Ezhuthachan, "Solution processable PEDOT: PSS/multiwalled carbon nanotube composite films for flexible electrode applications," *Phys. Status Solidi (A)*, Jun. 2018, Art. no. 1701003.

Yogeenth Kumaresan received the B.Eng. degree in electronic and communication engineering from Anna University, India, the master's degree in nanotechnology from Amity University, India, and the Ph.D. degree in flexible and stretchable electronic devices from the Gwangju Institute of Science and Technology, South Korea, in 2019. He is currently a Postdoctoral Researcher with the Bendable Electronics and Sensing Technology (BEST) Research Group, University of Glasgow, U.K. His research interests include physical sensors for soft robotics, MOSFETs, ultra-thin chips, and flexible/stretchable electronics,

Oliver Ozioko received the B.Eng. degree in electronic engineering from the University of Nigeria Nsukka, the master's degree in electronic/electrical engineering from the Federal University of Technology Owerri, Nigeria, in 2012, and the Ph.D. degree from the University of Glasgow, U.K., in 2019. He is currently a Postdoctoral Researcher with the Bendable Electronics and Sensing Technologies (BEST) Group, University of Glasgow. His current research interests include electronic skin, haptics, soft robotics, wearable tactile sensors and actuators for application in robotics and assistive technologies.

Ravinder Dahiya (Fellow, IEEE) is a Professor of Electronics and Nanoengineering with the University of Glasgow, U.K. He is also the Leader of the Bendable Electronics and Sensing Technologies (BEST) Research Group. His group conducts fundamental and applied research in flexible and printable electronics, tactile sensing, electronic skin, robotics, and wearable systems. He has authored more than 350 research articles, seven books, and 15 submitted/granted patents. He has led several international projects. He has been the President-Elect since 2020 and a Distinguished Lecturer of the IEEE Sensors Council. He is serving on the Editorial Boards of the Scientific Report. He was also on the Editorial Boards of IEEE SENSORS JOURNAL from 2012 to 2020, and IEEE TRANSACTIONS ON ROBOTICS from 2012 to 2017. He was the Technical Program Co-Chair of IEEE SENSORS 2017 and IEEE SENSORS 2018 and has been the General Chair of several conferences, including IEEE FLEPS in 2019, 2020, and 2021, which he founded in 2019. He holds the prestigious EPSRC Fellowship and received in past the Marie Curie and Japanese Monbusho Fellowships. He has received several awards, including the 2016 Microelectronic Engineering Young Investigator Award (Elsevier), the 2016 Technical Achievement Award from the IEEE Sensors Council, and nine best paper awards as author or coauthor in International Conferences and Journals.